RSC Advances

PAPER

Cite this: *RSC Adv.*, 2024, **14**, 19134

A multifunctional thermosensitive hydrogel based on phototherapy for promoting the healing of dental extraction wounds†

Shurui Shi, ‡*[a] Yunhan Chang,‡[a] Kaiyu Fu,[b] Ning Fu,[c] Xin Hu,[a] Borui Zhao,[a] Bo Chen,[a] Xinyue Yun[a] and Enyu Shi*[a]

Post-extraction wound infections are a common complication of dental extractions. More specifically, infection in the alveolar socket after tooth extraction accelerates the resorption and destruction of the alveolar bone, and ultimately affects the final restoration results. Currently, the main clinical treatment approaches applied to the socket after tooth extraction include mechanical wound debridement, chemical rinses (*e.g.*, chlorhexidine), filling of the extraction socket with absorbent gelatin sponges, and the systemic application of antibiotics. However, these traditional treatment modalities have some limitations and their therapeutic effects are unsatisfactory. In this study, a phototherapeutic temperature-sensitive hydrogel material was constructed for injection using a tea polyphenol (TP)-modified poly-*N*-isopropylacrylamide (PNIPAM) hydrogel skeleton loaded with the photosensitiser indocyanine green (ICG). The resulting PNIPAM-TP/ICG system exhibited an excellent injectability and temperature-sensitive properties. In addition, it stopped haemorrhaging and acted as a wound astringent. The hydrogel steadily released ICG into the oral environment to exert photothermal/photodynamic effects along with synergistic antibacterial and anti-inflammatory properties when combined with tea polyphenols. *In vivo* experiments demonstrated that the application of PNIPAM-TP/ICG to infected dental extraction wounds in rats rapidly stopped the bleeding and accelerated wound healing. Overall, this study describes a drug-loaded, temperature-sensitive hydrogel for the treatment of open wound infections, and shows promise as a reference for the treatment of tooth extraction wounds.

Received 30th April 2024
Accepted 3rd June 2024

DOI: 10.1039/d4ra03211j

rsc.li/rsc-advances

Introduction

Post-extraction wound infection is a common complication of tooth extraction and usually causes severe pain, leading to prolonged wound healing and complications, such as tissue necrosis and sepsis. The most common causes of such infections are periodontal disease in the localised area of the affected tooth, and the inability to maintain postoperative cleanliness around the wound. Open wounds are extremely prone to bacterial infections, which in turn cause sustained inflammatory responses that delay wound healing. Susceptibility to infection is also determined by the patient's age, hormone levels, stress levels, the presence or absence of diabetes, and any other factors that may affect the immune system.[1] It is well known that the establishment of an uncontrollable infection in the alveolar socket after tooth extraction accelerates resorption and destruction of the alveolar bone, in addition to increasing the risk of dry socket syndrome.[2,3] Significant research focus has therefore been placed on reducing the risk of postoperative infection after tooth extraction. Indeed, the ability to quickly and effectively treat postoperative wounds to achieve antibacterial and haemostatic effects is essential for wound healing. Currently, the majority of clinical approaches for the treatment of dental extraction sockets include mechanical debridement, treatment with chemical rinses (*e.g.*, chlorhexidine), filling of the extraction sockets with absorbent gelatin sponges, and the systemic application of antibiotics.[4,5] However, these approaches have various disadvantages. For example, mechanical debridement is generally incomplete, while chemical rinses are removed easily from the wound and can cause irritation. In addition, absorbent gelatin sponges often cannot adapt their shapes to the extraction socket, and such sponges lack antibacterial components.[6] Furthermore, the systemic application of antibiotics does not prevent bleeding, pain, or swelling, and it also tends to cause the development of systemic antibiotic resistance.[2,7] It is therefore of high clinical significance to explore new types of filling materials for extraction

[a]*School and Hospital of Stomatology, Tianjin Medical University, Tianjin Key Laboratory of Oral Soft and Hard Tissues Restoration and Regeneration, Tianjin 300070, China. E-mail: ssrwade@sina.cn; shienyukeyan@163.com*

[b]*Department of Pediatric Dentistry, Tianjin Stomatological Hospital, School of Medicine, Nankai University, Tianjin, 300041, China*

[c]*Jingnan Medical Area, Chinese PLA General Hospital, Beijing, 100071, China*

† Electronic supplementary information (ESI) available. See DOI: https://doi.org/10.1039/d4ra03211j

‡ S. S. and Y. C. contributed equally to this work.

sockets to overcome the problems associated with traditional treatment methods. Such materials should possess a number of characteristics, including self-adaptation to the shape of the extraction socket, a haemostatic effect and the ability to promote wound healing, a drug-loading and release ability, good antibacterial and anti-inflammatory properties, and ease of clinical practice.

Hydrogel materials are cross-linked polymer networks that exhibit high water absorption capacities and the ability to maintain the integrity of the material structure. Consequently, hydrogels have been employed to fulfil the needs of several applications, including those of the electrical, chemical, and wastewater treatment fields. Due to their excellent biocompatibilities and adjustable physical properties, hydrogels have also been extensively studied for use in biomedical applications.[8–10] For example, hydrogel materials can adsorb wound exudates, provide good haemostasis, and fill irregularly shaped wounds; thus, their application as wound dressings[11] has great potential. Currently, a variety of hydrogel materials that can alter their morphologies according to changes in the external environment (*e.g.*, temperature, pH, enzymes, and light) have been successfully developed and used to achieve the selective release of drugs at the sites of wounds.[12–14] In recent years, the development of novel hydrogel materials exhibiting a range of functions has gained increasing research attention. In this context, poly-*N*-isopropylacrylamide (PNIPAM) is a water-soluble polymeric material with thermosensitive properties, which usually undergoes a solid–liquid phase transformation when the environmental temperature reaches its lowest critical solubility temperature of ~32 °C. Because this temperature is very close to the physiological temperature of the human body, PNIPAM has been widely used in the synthesis of thermosensitive drug-loaded hydrogels bearing different functional components through the effective loading of multiple drugs and protein molecules.[15]

Tea polyphenols (TPs) are non-toxic and biocompatible natural polyphenolic compounds that are generally not susceptible to drug resistance. TPs are known for their long-term antioxidant effects[16] and the wide-spectrum antibacterial, anti-inflammatory, and haemostatic abilities[17] that promote wound site healing.[18–20] It has been shown that macrophage-mediated inflammation at wound sites can be regulated by the Notch signalling pathway;[21] TPs regulate *in vivo* wound healing by targeting this pathway, thereby inhibiting macrophage aggregation at the wound sites, and suppressing the inflammatory response.[22] In one study, Basiricò *et al.* confirmed that TPs improve the local inflammatory states of tissues by promoting expression of the anti-inflammatory factor IL-10.[17] In addition, the presence of abundant phenolic groups in the molecular structures of the TPs can lead to hydrogen bond formation with hydrophilic polymers, such as hyaluronic acid (HA), polyvinyl alcohol (PVA), and gelatin,[23,24] thereby generated cross-linked structures. The combination of TPs with hydrogel materials therefore has the potential to enhance the mechanical properties of hydrogel materials,[25] increase the haemostatic efficacy of the hydrogel, promote wound contraction, accelerate wound vascularisation, and enhance collagen generation, thereby promoting wound healing.[20]

Photothermal therapy (PTT) uses photothermal agents to generate heat under the irradiation of near-infrared (NIR) light at specific wavelengths. This can promote the local destruction of bacterial cell membranes, in addition to the denaturing of intracellular bacterial proteins. Importantly, PTT can be easily controlled in terms of its duration and range, leading to a low toxicity, good selectivity, limited drug resistance, and reduced levels of damage to normal tissues. Consequently, PTT has many advantages and broad application prospects for use in broad-spectrum antibacterial therapies. In this context, indocyanine green (ICG) is an NIR fluorescent dye that has been approved by the United States Food and Drug Administration (US FDA) for medical diagnosis. It belongs to the tricarbocyanine dye family and exhibits a certain degree of water solubility.[26] Compared to other photosensitisers, ICG presents certain advantages in terms of its therapeutic efficacy and clinical safety. In practical applications, ICG is often combined with various carriers to enhance its stability. Notably, ICG can also be used in photodynamic therapy (PDT) due to its effective absorption of NIR irradiation to generate antibacterial reactive oxygen species (ROS), which also play a role in anti-inflammatory responses. The microbial killing effect of ICG is therefore mainly derived from its photodynamic and photothermal effects; by absorbing laser light at specific wavelengths, ICG can generate thermal energy and denature bacterial proteins to exert its microbicidal effects.[27] The inhibitory effect of this compound on bacteria has found to increase gradually with an increasing ICG concentration and a longer laser irradiation time. In this context, Pourhajibagher *et al.*[28] reported that in the presence of 1000 μg mL^{-1} ICG, NIR laser irradiation at 62.5 J cm^{-2} for 2 min led to 93.7% cell death for *Porphyromonas gingivalis*. An analogous result was reported by Fekrazad *et al.*,[29] who described 96.68% cell death of *Porphyromonas gingivalis* under similar conditions. It is known that bacterial biofilms exhibit resistance to antibacterial drugs, thereby increasing the concentration of photosensitisers and prolonging the duration of laser irradiation.[30] However, the instability and aggregation-induced self-burst effect of ICG in solution pose challenges to its application. To address the inherent defects of ICG and optimise its performance, various ICG-containing drug formulations and carrier systems have been developed.[31,32]

Thus, to expand on these previous works, we herein report the development of a new and improved filler material for application in dental extraction sockets. More specifically, a thermosensitive hydrogel material suitable for application in PTT/PDT is prepared by the incorporation of ICG and TPs into the cross-linked network of PNIPAM (*i.e.*, PNIPAM-TP/ICG). Subsequently, the antibacterial, haemostatic, and anti-inflammatory properties of the developed hydrogel are evaluated, and its potential for promoting wound healing is examined (Fig. 1).

Materials and methods

Materials

PNIPAM was purchased from RHAWN company (Shanghai, China). Indocyanine Green (ICG) was bought from J&K Scientific (Beijing, China). The TPs were acquired from Meilun

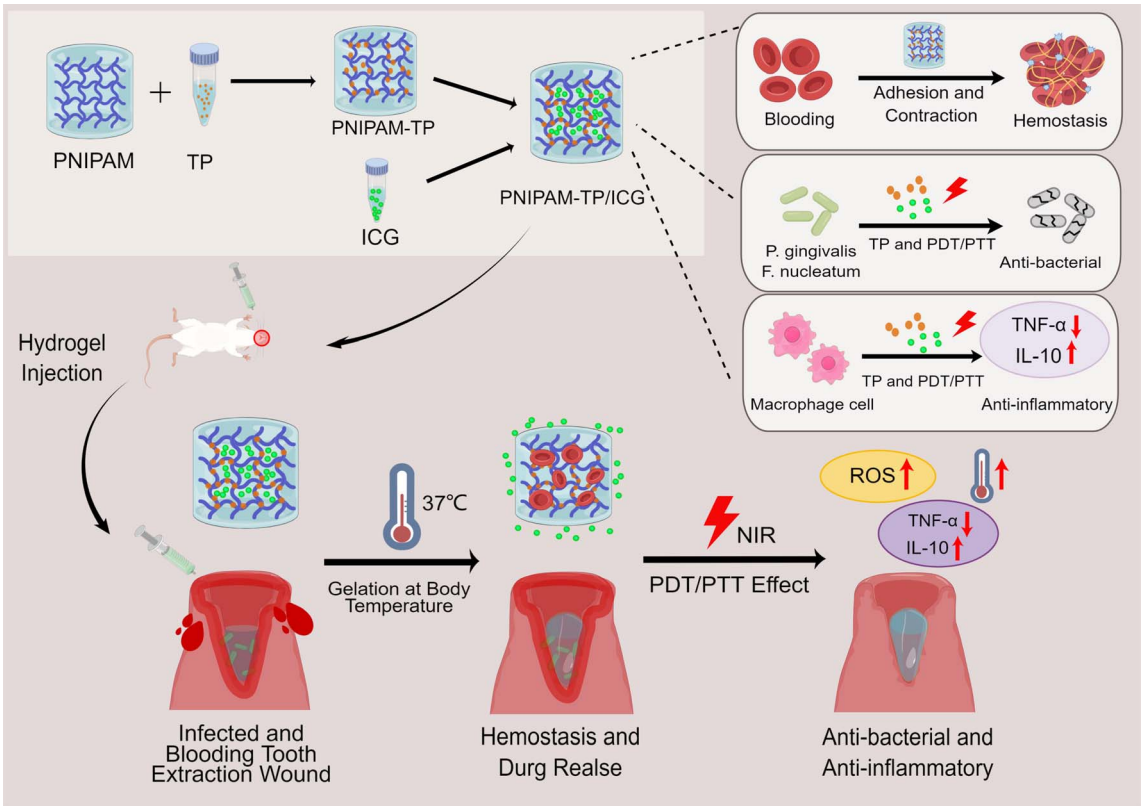

Fig. 1 Diagrams of the formation of PNIPAM-TP/ICG hydrogel and the mechanisms of accelerating wound healing effect (By Figdraw).

Biology and Technology (Dalian, China). 9,10-anthracenediyl-bis(methylene)dimalonic acid (ABDA) was purchased from Sigma-Aldrich (St Louis, MO, USA).

Bacterium and animals

The *Porphyromonas gingivalis* (*P. gingivalis*, Pg) *Fusobacterium nucleatum* (*F. nucleatum*, Fn) strain was obtained from the BeNa culture collection and cultured in brain heart infusion (BHI) broth medium (Solarbio, Beijing, China) under anaerobic conditions at 37 °C. Female Sprague–Dawley (SD) rats, weighing 160 ± 20 g, were purchased from Vital River Laboratory Animal Technology Company (Beijing, China). Bleeding and infection models of tooth extraction were established. The SD rats were anesthetized with isoflurane by inhalation, and the right maxillary anterior teeth were extracted to establish the extraction wound model. All animal experiments were conducted in accordance with the protocol approved by the Animal Protection and Use Committee of Tianjin Medical University.

Synthesis of the PNIPAM-TP/ICG hydrogel

To conjugate the TPs to the PNIPAM hydrogel, PNIPAM (300 mg) was dissolved in *N*,*N*-dimethylformamide (DMF, 4 mL) and placed in an ultrasonic shaker in a water bath at 4 °C for 10 min until a homogeneous solution was formed. Subsequently, a 2 mg mL^{-1} solution of TP-DMF was prepared, and an aliquot (100 μL) was added to the above PNIPAM-DMF solution. After stirring magnetically at 600 rpm for 1 h to obtain a homogeneous solution, an ICG-DMF solution (25 μL, 2 mg mL^{-1}) was added to give a TP/ICG mass ratio of 4 : 1. After stirring at 4 °C for a further 1 h, the resulting solution was placed in a vacuum drying oven at 60 °C for 24 h. Subsequently, DDW (1 mL) was added, and the mixture was allowed to stand at 4 °C for 24 h to obtain the desired PNIPAM-TP/ICG hydrogel. All operations involving ICG were performed in the absence of light.

Characterisation of the PNIPAM-TP/ICG hydrogel

The surface morphology of the PNIPAM-TP/ICG hydrogel was observed by scanning electron microscopy (SEM). The absorbance values of the PNIPAM, ICG, TP, PNIPAM-TP, and PNIPAM-TP/ICG species were measured at different wavelengths using ultraviolet-visible (UV-vis) spectrophotometry. Absorbance–wavelength curves were plotted to verify the successful preparation of the desired materials. The sizes and size distributions of the PNIPAM-TP and PNIPAM-TP/ICG hydrogels were measured using an automatic particle detector. A modular compact rheometer (Anton Paar GmbH, Graz, Austria) was used to evaluate the rheology of the PNIPAM-TP/ICG hydrogel.

In vitro drug release study

The *in vitro* release of ICG from the PNIPAM-TP/ICG hydrogel was measured in a phosphate buffered saline (PBS) release medium at pH 7.4 and 6.8 using a dynamic dialysis approach.

For this purpose, the PNIPAM-TP/ICG hydrogel (2 mL) was transferred into a dialysis bag with a molecular weight cut-off (MWCO) of 500 Da. The hydrogel was dispersed in the release medium, and then placed in a 37 °C constant temperature shaker. After performing dialysis for the scheduled times, aliquots were removed for analysis, and equal volumes of fresh release medium were added. The amount of ICG released was determined using UV-vis spectrophotometry at 780 nm.

In vitro assessment of the PTT/PDT performance

The PTT performance of the PNIPAM-TP/ICG hydrogel was evaluated using thermal distribution images of the hydrogel. Laser irradiation (2 W cm^{-2}) was applied to the hydrogel using an 808 nm laser transmitter for 10 min, during which time, a fixed interval was set. The PDT performance of the PNIPAM-TP/ICG hydrogel was evaluated by detecting the generation of ROS under laser irradiation. More specifically, the hydrogel was placed in a UV-vis spectrophotometer for zero adjustment. Subsequently, 100 μM of the ABDA reactive oxygen probe was added to the hydrogel. Laser irradiation (2 W cm^{-2}) was applied to the hydrogel using an 808 nm laser transmitter for 10 min, during which time, the absorbance at 380 nm was detected by UV-vis spectrophotometry at 2 min intervals.

In vitro antibacterial tests

The synergistic antibacterial activity of the PNIPAM-TP/ICG hydrogel-mediated combination treatment was assessed in Pg and Fn by measuring the optical density at 600 nm (OD_{600}). The bacterial density of the Pg solution was adjusted to 1×10^4 CFU mL^{-1}, transferred to 96-well plates, and incubated for 24 h. The treatment groups consisted of the PBS control, PNIPAM, free ICG, PNIPAM-TP, PNIPAM-TP/ICG, free ICG + laser, and PNIPAM-TP/ICG + laser groups. The concentrations of ICG employed were 0, 3, 6, 9, 12, and 15 μg mL^{-1}, while the TP concentrations were 0, 12, 24, 36, 48, and 60 μg mL^{-1}. In the laser irradiation group, each group of samples was incubated for 1 h and then irradiated for 10 min using an 808 nm wavelength laser transmitter with an intensity of 2 W cm^{-2}. Subsequently, 4 h after treatment, the absorbance of each well was measured at 600 nm using a UV-vis spectrophotometer.

The synergistic antibacterial activity of the PNIPAM-TP/ICG hydrogel-mediated combination treatment was also evaluated using live/dead cell staining. For this purpose, the Pg and Fn bacterial fluids were seeded into 12-well glass culture plates, incubated for 4 days, treated in the same manner as described above, and then incubated for another 24 h. Finally, the treated bacteria were stained using the live/dead cell staining kit according to the manufacturer's protocol, and were observed under a fluorescence microscope. The intracellular ROS generation of Pg and Fn triggered by triggered by various treatments was detected by flow cytometry using DCFH-DA as a fluorescence probe. Briefly, the bacteria were seeded into 12-well plates at a density of 1×10^4 CFU mL^{-1} and cultured for 24 h. Next, the bacteria were incubated separately with PNIPAM, PNIPAM-TP, PNIPAM-TP/ICG and free ICG for 1 h. After this, some groups of bacteria were exposed to 808 nm laser irradiation for 10 min with an intensity of 2 W cm^{-2}. After 4 h of treatment, the bacteria were processed with 20 μmol L^{-1} of DCFH-DA for 30 min according to the manufacturer's protocol, and the intracellular fluorescence signals DCF were detected using flow cytometry assay.

In vivo haemostatic effect

A bleeding model of dental extraction trauma was established in SD rats to observe the haemostatic effects of the hydrogel *in vivo*. For this purpose, female SD rats (280–320 g body mass) were randomly divided into five groups ($n = 3$), namely the PBS control, PNIPAM, PNIPAM-TP, PNIPAM-TP/ICG, and PNIPAM-TP/ICG + laser groups. After anaesthesia by isoflurane inhalation, the right maxillary anterior teeth of the SD rats were extracted using microinvasive treatment. Following treatment of the extraction wound according to the defined group, an absorbent paper point (GAPADENT, China) was placed at the extraction wound and maintained for 5 s to wet the paper tip by active bleeding through siphoning. This step was carried out to characterise the amount of bleeding and record the time of haemostasis.

Subsequently, the hydrogel material in the extraction wound was removed and fixed with a 2% glutaraldehyde solution for 4 h, after which 75% ethanol, 85% ethanol, 95% ethanol, anhydrous ethanol I, and anhydrous ethanol II were sequentially applied for 15 min each to perform gradient dehydration. The hydrogel was then rinsed with *tert*-butanol and replacement. The mixture was then pre-cooled and dried in a lyophiliser for 24 h. Adsorption of blood cells onto the PNIPAM-TP/ICG hydrogel was observed using SEM.

In vivo wound healing tests

After anaesthesia by isoflurane inhalation, the right maxillary anterior teeth of the SD rats were extracted; the grouping was as described in Section 2.6. In this case, the endotoxin solution (50 μL) containing lipopolysaccharide (0.1 μg) was injected into the extraction socket. Subsequently, PBS (100 μL) or an equal volume of the hydrogel ($n = 3$) was injected into the extraction socket, and the laser group was irradiated using an 808 nm wavelength laser transmitter (2 W cm^{-2}) for 10 min. Photographic images were captured to examine the healing status of each wound on days 0, 3, and 7 after tooth extraction. The hydrogel was replaced every 2 days until the end of the experiment.

Determination of the anti-inflammatory efficacy of the hydrogel

The anti-inflammatory efficacy of the PNIPAM-TP/ICG hydrogel was evaluated in the SD rat model. After anaesthesia by isoflurane inhalation, the right maxillary anterior teeth of the SD rats were extracted. The extraction sockets were then scratched, and the exudates were collected and stored at 4 °C. Subsequently, aliquots (200 μL) of the Pg and Fn bacterial solutions was injected into the extraction sockets, and after 2 h, the sockets were scratched once again, and the exudates were collected and stored at 4 °C. The rats were then randomly

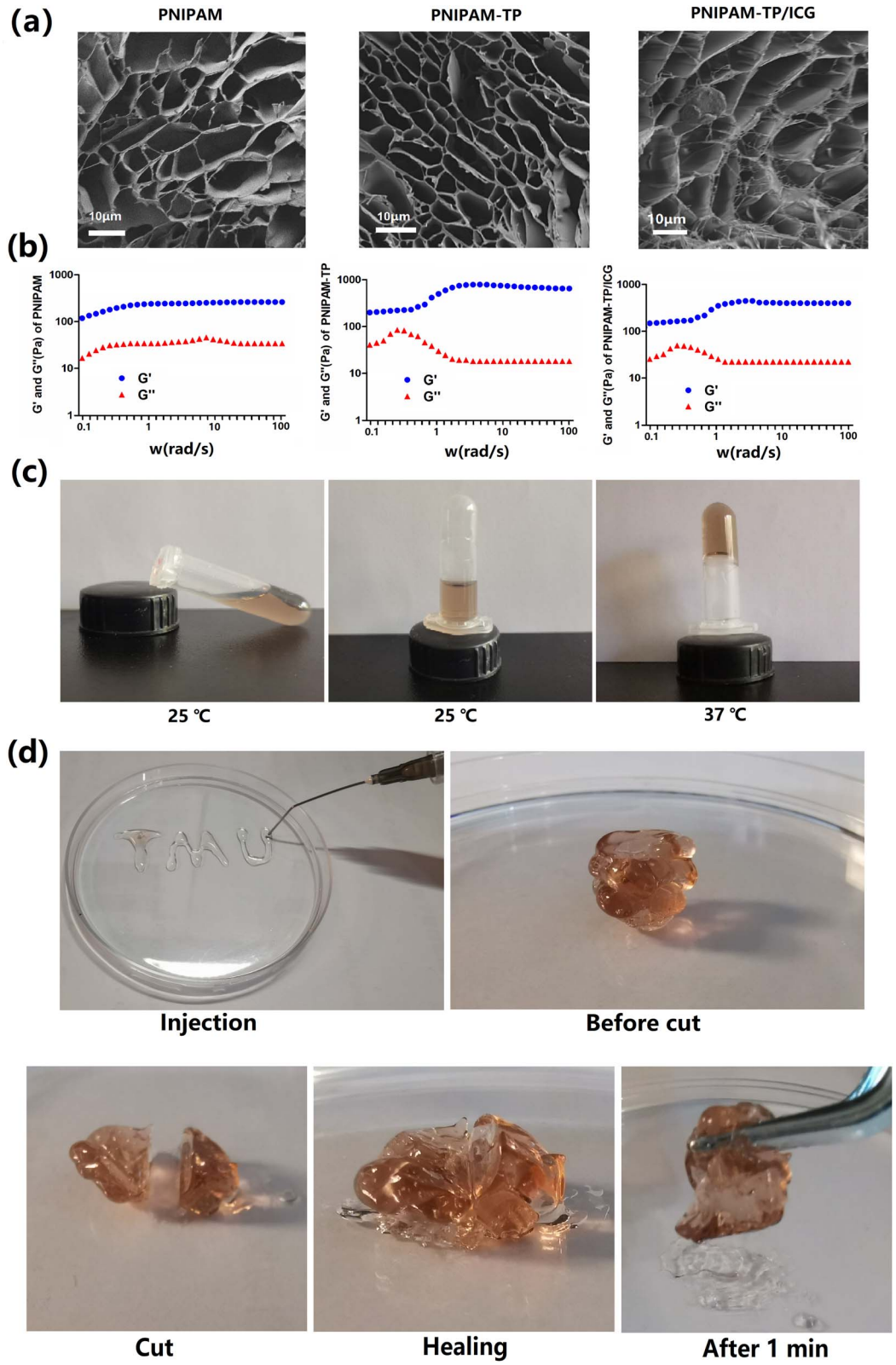

Fig. 2 Dynamic functions, microstructure and rheological characteristics of hydrogels. (a) Scanning electron microscopy images of PNIPAM, PNIPAM-TP, and PNIPAM-TP/ICG hydrogels. (b) Storage modulus (G') and loss modulus (G'') of PNIPAM, PNIPAM-TP, and PNIPAM-TP/ICG hydrogels as a function of frequency. (c) Fluidity and (d) injectability of PNIPAM-TP/ICG hydrogel materials at room temperature and in a 37 °C environment.

divided into five treatment groups (*i.e.*, the PBS, PNIPAM, PNIPAM-TP, PNIPAM-TP/ICG, and PNIPAM-TP/ICG + laser groups) based on an ICG concentration of 50 μg mL^{-1} and a TP concentration of 200 μg mL^{-1}. Following treatment and allowing the extraction sockets to stand for 12 h, the sockets were scratched and the exudates were collected and stored at 4 °C. An aliquot (100 μL) of each extraction socket exudate was collected for determination of the TNF-α and IL-10 levels using an ELISA kit. Similarly, the total protein concentrations were determined using a bicinchoninic acid kit. After several days of treatment, all the rats were sacrificed, and the main organs were separated for further examination. Briefly, the samples were fixed with 4% paraformaldehyde, embedded with paraffin, and cut into 5 μm sections, and then stained with hematoxylin & eosin (H&E) for histopathological analysis.

Statistical analysis

All measurements were carried out at least in triplicate and all values are indicated as the mean ± standard deviation (SD). Statistical analysis was carried out using Student's *t*-test, wherein a p value < 0.05 represented a statistical difference.

Results and discussion

Synthesis and physical properties of the PNIPAM-TP/ICG hydrogel

The TPs were complexed with PNIPAM *via* a layer-by-layer assembly approach in DMF to generate a stable three-dimensional network skeleton structure. Subsequently, ICG was loaded onto this skeleton, and the microstructures of the corresponding hydrogels were visualised using SEM. As shown in Fig. 2a, all hydrogels were porous, with pore sizes ranging from 5 to 50 μm. Notably, the introduction of TPs had no influence on the microstructural features of the hydrogels. In contrast, the loaded ICG drug particles were clearly observed in the pore structure of the PNIPAM-TP/ICG hydrogel.

To evaluate the mechanical properties of the PNIPAM-TP/ICG hydrogel, the storage modulus (G') and loss modulus (G'') were determined using oscillatory shear measurements. As shown in Fig. 2b, all three groups of materials remained elastic ($G' > G''$) in the range of 0.1–100 rad s^{-1} at 37 °C, which is consistent with the typical behaviour of gel materials.[33] The complexation of TPs with PNIPAM resulted in elevated G' and G'' values, demonstrating that the mechanical properties of the hydrogels had been improved.[25] It was also determined that the introduction of ICG played no role in altering the mechanical properties of hydrogels.

Moreover, it was deduced that the prepared PNIPAM-TP/ICG hydrogel material retained the thermosensitive properties of the original PNIPAM hydrogel scaffold. As shown in Fig. 2c, the modified hydrogel exhibited a good fluidity at room temperature, and was able to undergo a liquid-to-gel transition with a significant change in fluidity when the temperature reached 37 °C. This property facilitates the application of the hydrogel in post-extraction wound fixation, and indicates its potential to exhibit a sustained drug release performance.

To demonstrate the injectability of the hydrogel, a needle was used to deliver the hydrogel in the formation of the letters "TMU", as shown in Fig. 2d. In addition, the self-healing properties of the hydrogel were examined. More specifically, after warming and gelatinising the hydrogel, a circular segment was cut from the middle, and the two parts of the hydrogel were docked together and allowed to stand for 10 min. After this time, the structural strength of the hydrogel was completely restored, and the healed gel could be using tweezers.

Characterisation of the PNIPAM-TP/ICG hydrogel

To assess the size changes between hydrogel and drug loading hydrogel, we measured the sizes and size distributions of PNIPAM hydrogel and PNIPAM-TP/ICG hydrogel using dynamic light scattering. As shown in Fig. 3a, the particle size of the PNIPAM hydrogel was determined to be ~283.7 nm with a relatively narrow size distribution. Due to the complex internal network structures of PNIPAM hydrogel, the size distribution exhibited 2–3 absorption peaks. After loading both the TP and ICG components, the particle size increased slightly to 308.1 nm (Fig. 3b). However, the polydispersity index (PDI) remained relatively constant at ~0.3, thereby indicating the complexation of TP and the loading of ICG almost did not change the overall structure of the hydrogel.

The drug loading capabilities of the hydrogel specimens were also evaluated using UV-vis spectrophotometry. The absorbance values of the PNIPAM, ICG, TP, PNIPAM-TP, and PNIPAM-TP/ICG samples were measured at different wavelengths, and their corresponding absorbance–wavelength curves were plotted, as shown in Fig. 3c. Characteristic UV absorption peaks of were observed for the TPs and ICG at 275 and 780 nm, respectively, and it was found that the UV absorption curves of the PNIPAM-TP/ICG hydrogel contained the characteristic absorption peaks corresponding to both the TPs and ICG. The maximum absorption peaks observed for equal concentrations of ICG in the free state and in the hydrogel were almost identical, indicating that the optical properties of ICG did not change significantly during its incorporation into the hydrogel. However, a red shift was observed for the characteristic ICG peaks upon formation of the PNIPAM-TP/ICG hydrogel, confirming the successful wrapping effect of the PNIPAM-TP/ICG hydrogel on the ICG molecules. The concentration–absorbance curves of the TP and ICG solutions were obtained at various dilutions by measuring the absorbances at 275 and 780 nm, respectively.

The drug-loaded hydrogel described herein was designed to treat infected extraction wounds by providing antibacterial and anti-inflammatory effects, which requires the rapid release of ICG. Thus, drug release from the PNIPAM-TP/ICG hydrogel was detected in different environments using the dynamic dialysis approach. The absorbance of the release solution at each time point was observed at 780 nm, and the ICG concentration in each release solution was determined using the concentration–absorbance curves described above. The drug release rate was calculated, and the release curves were plotted, as shown in Fig. 3d. In a neutral environment (pH 7.4), ICG was released rapidly,

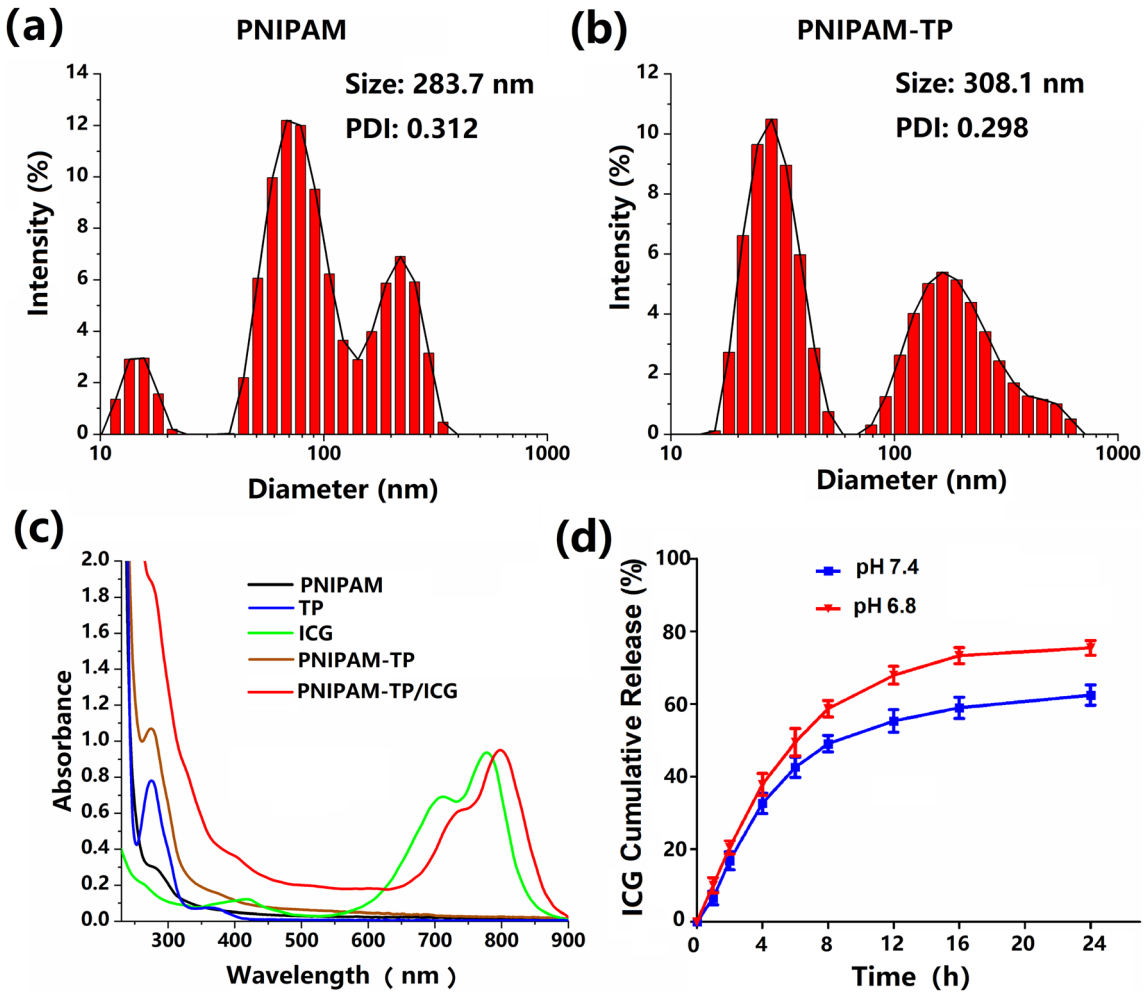

Fig. 3 Characterization of the PNIPAM-TP/ICG Hydrogel. Particle size distribution plots of (a) PNIPAM and (b) PNIPAM-TP/ICG. (c) UV-vis absorbance spectrum of PNIPAM, ICG, TP, PNIPAM-TP and PNIPAM-TP/ICG. (d) The release curves of ICG in different pH environments.

reaching 30% release after 4 h. Beyond this point, ICG release slowed, reaching ~60% after 24 h. In the simulated oral environment (pH 6.8), ~40% of the ICG was released after 4 h, and this increased significantly to ~80% after 24 h. These results clearly demonstrated that a higher ICG release rate was detected in the simulated oral environment (pH 6.8). The released ICG from hydrogel can better target bacteria that colonize the surface of the periodontal ligament, thus more sufficiently exerting the antibacterial effects through PTT/PDT efficacies. Notably, release of the TPs was not detected using this approach (detection wavelength = 275 nm), demonstrating that the TPs were tightly bound to the PNIPAM hydrogel backbone. The complexation of TP into hydrogel can significantly improve the mechanical properties, antibacterial ability, contractive and hemostatic effects of the hydrogel-TP, thus achieving the significant effects of anti-inflammatory and promoting wound healing.

In vitro PTT/PDT properties of the PNIPAM-TP/ICG hydrogel

The *in vitro* photothermal properties of the free ICG and the PNIPAM-TP/ICG hydrogel were investigated using an infrared imager, as shown in Fig. 4a. Under laser irradiation at a wavelength of 808 nm, PNIPAM-TP/ICG generated heat comparable to that of the free ICG, wherein the temperature initially increased rapidly prior to gradually stabilising during the 10 min irradiation time (Fig. 4b). In the case of the PNIPAM-TP/ICG hydrogel, the maximum absorption wavelength of ICG was closer to 808 nm owing to the red-shift phenomenon in its UV-vis spectrum. This result implies that the PNIPAM-TP/ICG hydrogel should be able to generate more heat than the free ICG. After 10 min of light exposure, the temperature of the hydrogel stabilised at ~55 °C, thereby demonstrating that this hydrogel possesses good photothermal properties.

It is well known that ABDA decomposes *via* a chemical reaction with photodynamically generated ROS, resulting in a decrease in the UV-vis absorbance that is positively correlated with the ROS content. Based on this principle, ABDA was used as a probe to investigate the *in vitro* photodynamic properties of the PNIPAM-TP/ICG hydrogel. As shown in Fig. 4c, the UV absorbance of ABDA in the wavelength range of 300–450 nm gradually decreased with an increasing irradiation time after addition of the PNIPAM-TP/ICG hydrogel. After 10 min of laser irradiation, the peak absorption of the PNIPAM-TP/ICG + laser

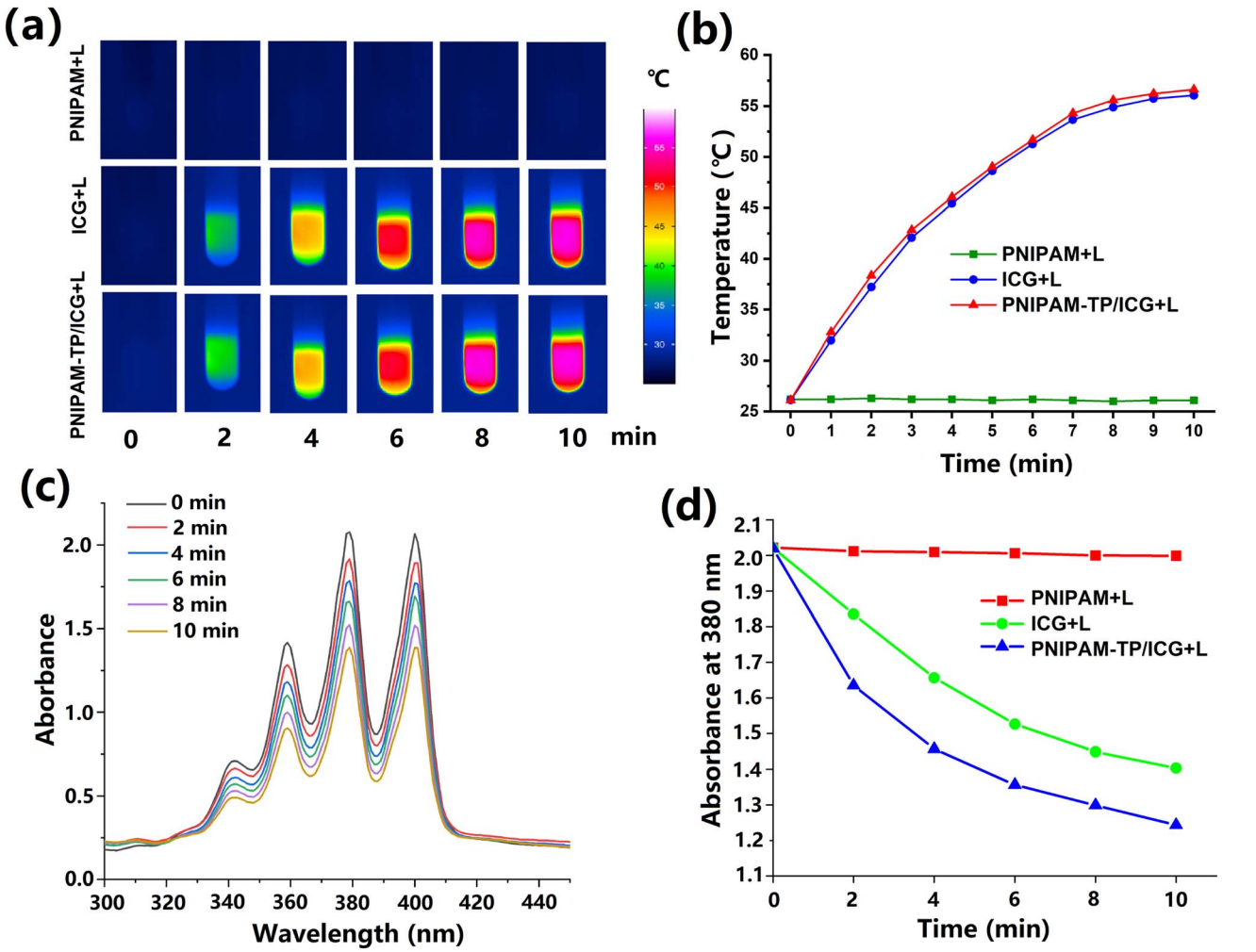

Fig. 4 *In vitro* PTT/PDT properties of the PNIPAM-TP/ICG hydrogel. (a) The infrared thermal images and (b) temperature changing curves of PNIPAM hydrogels, free ICG and PNIPAM-TP/ICG hydrogels during 10 min of laser irradiation. (c) UV-vis absorption spectrum of ABDA in PNIPAM-TP/ICG hydrogels during 10 min of laser irradiation. (d) Absorbance value changes at 380 nm of ABDA in PNIPAM hydrogels, free ICG and PNIPAM-TP/ICG hydrogels.

group at 380 nm decreased from 2.0 to 1.2, demonstrating that the PNIPAM-TP/ICG system generated ROS under laser irradiation conditions, and that the amount of ROS generation was greater than that of the free ICG (Fig. 4d). These results show that the photodynamic properties of ICG were not disturbed during hydrogel loading, but instead, they were enhanced. Moreover, the antioxidant effects of the TPs did not affect the photodynamic generation of ROS under the influence of ICG. This result lays the foundation for the photodynamic effects observed in subsequent studies.

In vitro antibacterial assay

The PNIPAM-TP/ICG hydrogel-mediated PTT/PDT effect was evaluated to determine the antibacterial effects of this system toward Pg and Fn. Before this, we firstly verified the bacteriostasis of laser irradiation itself, PNIPAM hydrogel and PNIPAM-TP hydrogel to evaluate the biosafety of laser irradiation itself and the hydrogels. As shown in Fig. S1,† laser irradiation itself, PNIPAM hydrogel combined with or without laser irradiation do not inhibit the growth of bacteria. Besides, the slight antibacterial effects between PNIPAM-TP hydrogel combined with laser irradiation and without laser irradiation almost identical. These results indicate the 2 W cm^{-2} intensity of laser irradiation possess no potential toxicity. As shown in Fig. 5a and b, the free ICG showed no antibacterial effect, whereas under laser irradiation at 808 nm, it was able to produce an antibacterial effect against Pg and Fn owing to its photothermal/photodynamic properties, and this effect was positively correlated with the ICG concentration. The ICG-containing hydrogel also exhibited similar antibacterial effects against Pg and Fn (Fig. 5c and d), suggesting that the hydrogel was able to release ICG and exert its PTT/PDT effects. In both the PNIPAM-TP and PNIPAM-TP/ICG hydrogel groups, the concentrations of Pg and Fn also tended to decrease with an increasing TP concentration, indicating that the TPs could exert an antibacterial effect, as described previously by Zheng *et al.*[34]

In addition, live/dead staining was employed after application of the different treatment approaches, wherein red and

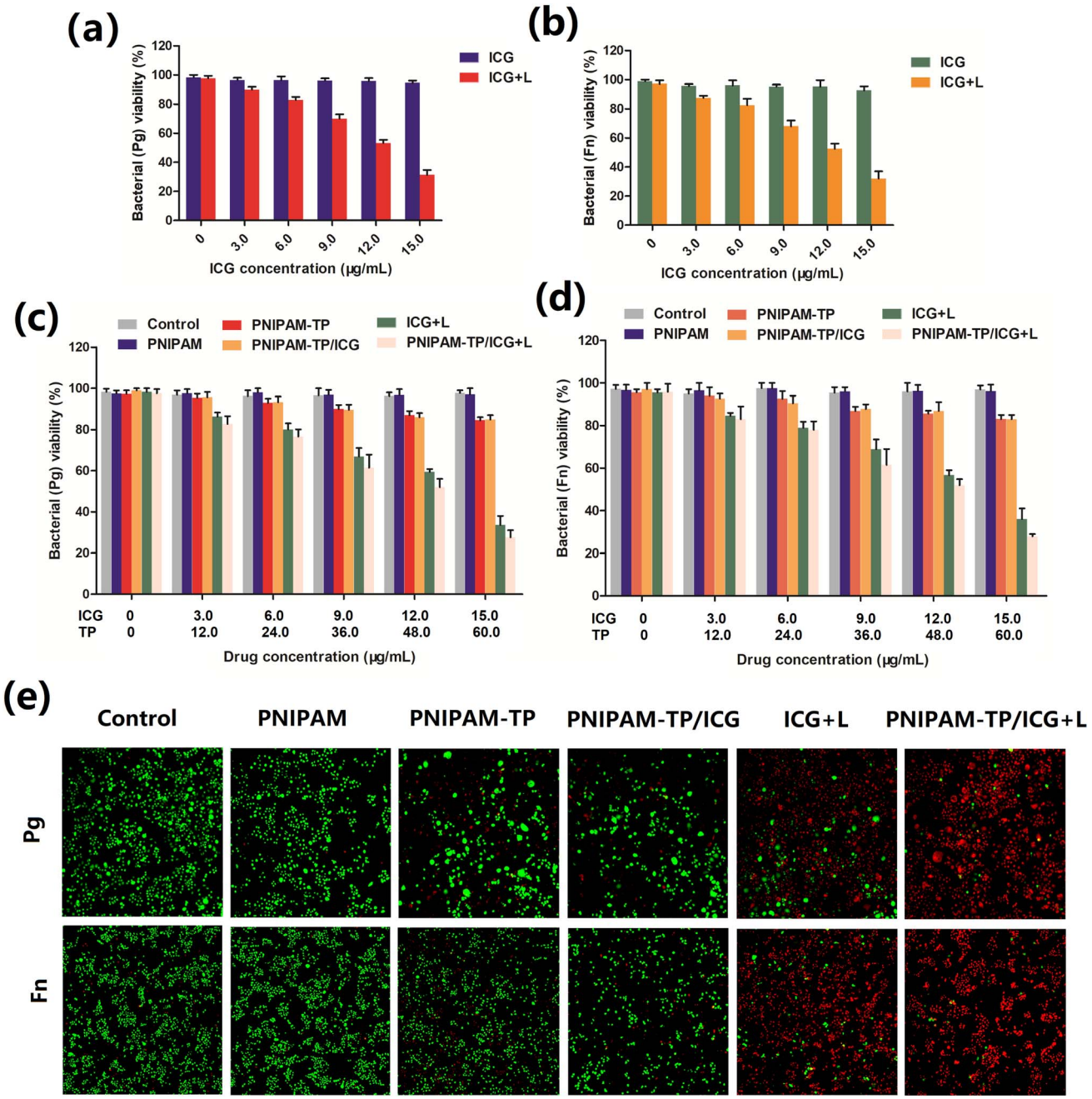

Fig. 5 Antibacterial properties of PNIPAM-TP/ICG hydrogels. Antibacterial activities of free ICG combined with or without laser irradiation in (a) *P. gingivalis* and (b) *F. nucleatum*. Antibacterial activities of various treatments in (c) *P. gingivalis* and (d) *F. nucleatum*. (e) Fluorescence microscopic images of the plaque biofilms stained with the Live/Dead staining kit.

green fluorescence correspond to the dead and live bacteria, respectively. As shown in Fig. 5e, the PNIPAM-TP and PNIPAM-TP/ICG groups exhibited some bactericidal effects, while the ICG + laser irradiation group showed an obvious bactericidal effect. Importantly, the PNIPAM-TP/ICG + laser group demonstrated a significantly enhanced bactericidal effect, which was superior to that of the ICG + laser group. In all other groups, low bacterial death rates were observed, thereby confirming that the PTT/PDT effect generated by the ICG component of the hydrogel can work in synergy with the TPs to exert enhanced antibacterial effects.

In addition, we also evaluated the intracellular ROS generation of Pg and Fn triggered by hydrogels combined with laser irradiation by flow cytometry using DCFH-DA as a fluorescence probe. DCFH-DA could be hydrolyzed by endogenous cell esterases to form nonfluorescent DCFH, which could rapidly oxidized into DCF possessing an intensive fluorescence under a sufficient ROS environment. Therefore, the fluorescent intensity of DCF is positively related to the ROS generation level. As shown in Fig. S2,† the DCF fluorescent intensities were weak after the mixed consortium (Pg and Fn) co-incubating with hydrogels and drug loading hydrogels. However, when ICG and

ICG contained hydrogels (PNIPAM-TP/ICG) were exposed to laser irradiation, the DCF fluorescent intensities significantly increased. The result indicated that the PNIPAM-TP/ICG combined with laser irradiation could generate large amounts of ROS in bacteria, thereby exerting its antibacterial effect.

In vivo haemostasis assay

Haemostasis is an essential step in the wound healing process, and controlling the active bleeding after tooth extraction surgery is a prerequisite for subsequent treatment.[35] As shown in Fig. 6a, a bleeding extraction wound model was created by extracting the right upper anterior teeth of SD rats in a minimally invasive manner. The bleeding volume was recorded by measuring the wetting length of the paper tip to evaluate the haemorrhagic ability of the hydrogel (Fig. 6b). Control rats that received no hydrogel treatment were found to experience a massive amount of blood loss, which was evident by the longer blood stain on the paper tip. In contrast, bleeding was significantly reduced after injection of the PNIPAM hydrogel into the extraction wound. This indicates that the PNIPAM hydrogel can adapt to the shape of the extraction socket, fill it tightly, and exhibit a good compressive haemostatic ability. In addition, as shown in Fig. 5A, when the PNIPAM-TP and PNIPAM-TP/ICG hydrogels were injected into the wound, the amount of bleeding was further reduced compared to the levels detected for the PNIPAM hydrogel. It was also found that the degree of haemorrhage was unrelated to the application of laser illumination. These observations confirmed that the combination of TPs with the hydrogel enhanced the haemostatic ability of the hydrogel material, reduced the bleeding volume, and shortened the clotting time (Fig. 6c and d).

Subsequently, the red blood cell (RBC) surface adhesion and morphology on the hydrogels was further investigated by SEM (Fig. 6e and f). It was found that a large number of RBCs adhered to the surfaces of both the PNIPAM and PNIPAM-TP/

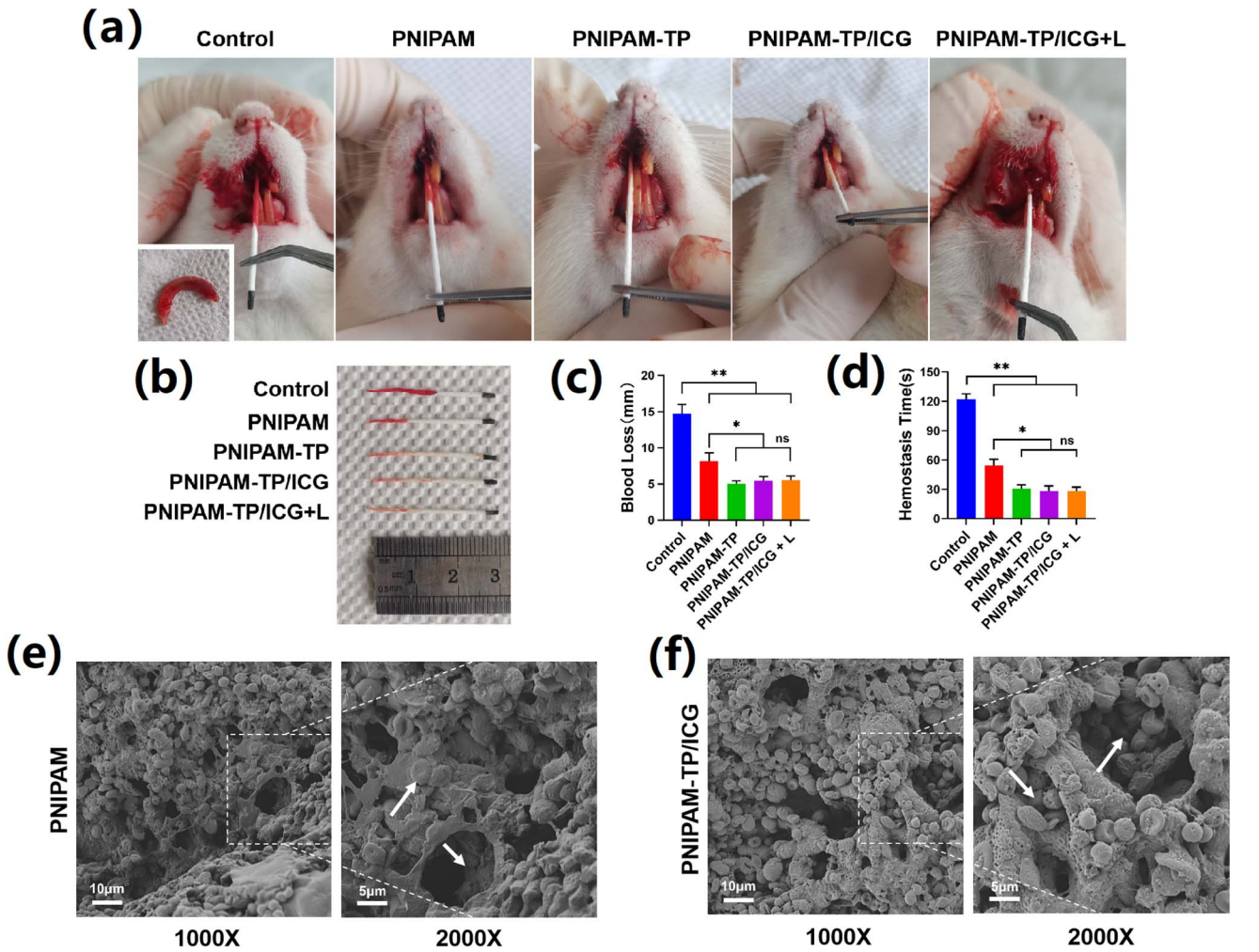

Fig. 6 Hemostatic properties of hydrogels. (a) Photographs of hemostasis in each group of the rat tooth extraction trauma bleeding model and the extracted teeth (inset). (b) Bleeding volume recorded after placing the paper tip at the tooth extraction wound for 5 seconds in each group. (c) Bleeding volume and (d) hemostasis time of the rat tooth extraction trauma bleeding model in each group. SEM observation of blood cell adhesion on the (e) PNIPAM and (f) PNIPAM-TP/ICG hydrogel. White arrows indicate red blood cells. Data are expressed as mean ± SD ($n = 3$). *P < 0.05 for comparison among different groups (one-way ANOVA), **P < 0.01 for comparison to the control (one-way ANOVA), ns indicates no statistical significance.

ICG hydrogels, and adherence was detected even within the deep hydrogel pores (Fig. 6e and f, white arrows). The experimental results described above demonstrate that the PNIPAM hydrogel, as a thermosensitive material, can be rapidly transformed into a gel state after injection into the body. Consequently, it can fill the extraction socket and achieve pressure haemostasis. Importantly, the loose and porous internal structure of the hydrogel can rapidly absorb large amounts of blood, combined with the astringent effects of TP, to exert an excellent haemostatic efficacy.

In vivo anti-inflammatory efficacy

To investigate the efficacy of hydrogel-mediated healing in the context of dental extraction wounds, an infected dental extraction wound model was constructed by the intravascular injection of LPS into minimally invasive dental extraction wounds in SD rats. As shown in Fig. 7a, the infected rat extraction wound models were divided into different treatment groups. The PNIPAM-TP/ICG + laser irradiation group exhibited the most rapid degree of wound healing, reaching almost 100% healing after 7 days. In the control and PNIPAM groups, yellow/white

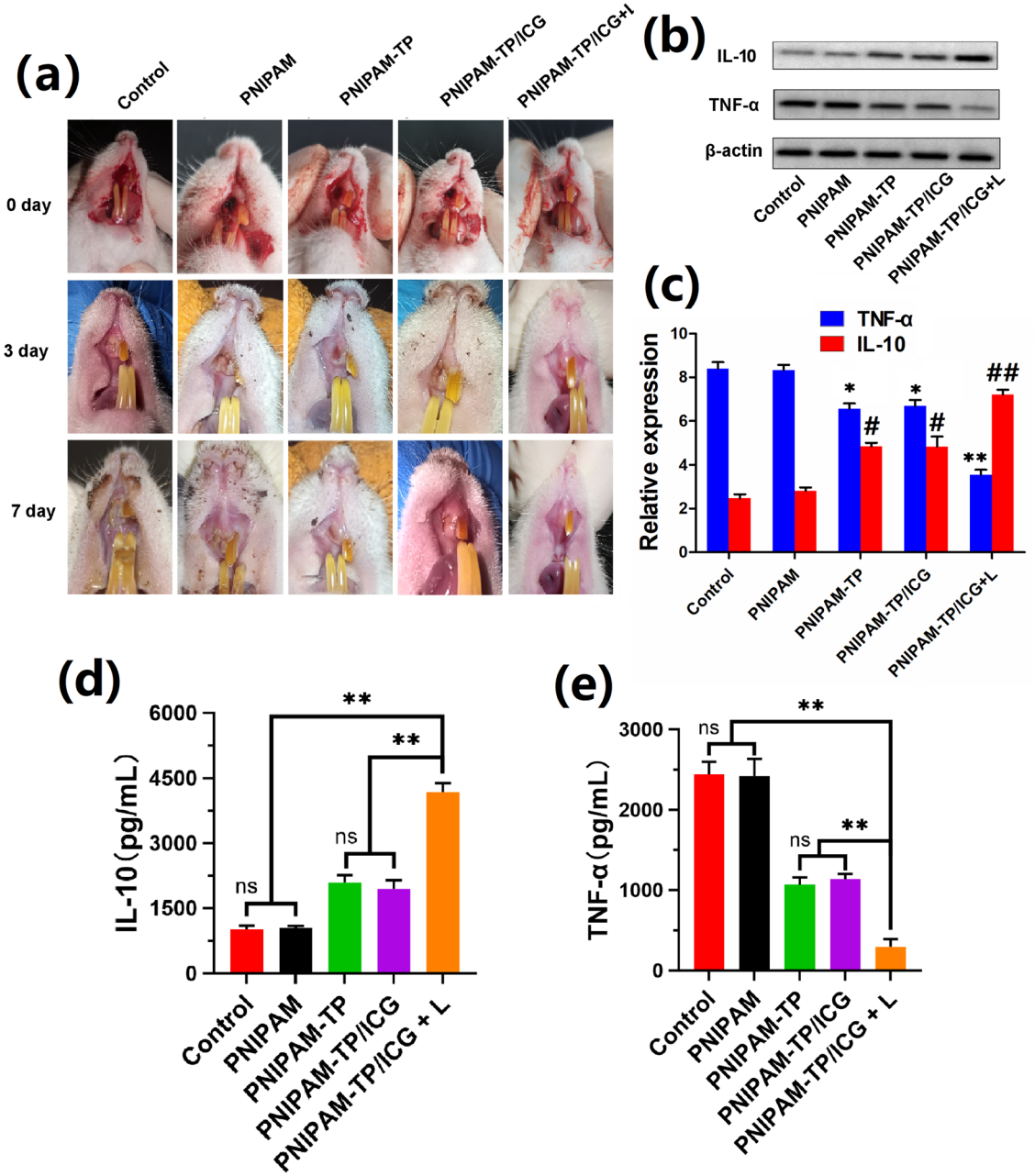

Fig. 7 *In vivo* assays to evaluate the effectiveness of hydrogels in the treatment of infected tooth extraction wounds in rats. (a) Photographs of tooth extraction wounds healing in rats at different time points after tooth extraction surgery. (b) Western blot analysis of the expression levels of IL-10 and TNF-α in each group. (c) Relative expression of IL-10 and TNF-α. The variations in the levels of IL-10 (d) and TNF-α (e) detected through ELISA assay. Data are expressed as mean ± SD ($n = 3$). * and # indicate $P < 0.05$ for comparison among different groups (one-way ANOVA), ** and ## indicate $P < 0.01$ for comparison among different groups (one-way ANOVA), ns indicates no statistical significance.

pseudo-membranes still existed on the wound surfaces after 7 days, and the surrounding gingival tissue exhibited obvious inflammatory features, such as redness and swelling. These results suggest that the PNIPAM-TP and PNIPAM-TP/ICG hydrogel groups healed more rapidly than the control and PNIPAM hydrogel groups, confirming the role of the TPs in promoting the healing of dental extraction wounds. These effects may be related to the antibacterial, anti-inflammatory, and wound-astringent effects of TP. After the addition of ICG, the PDT/PTT effect generated under laser irradiation further promoted the antibacterial and anti-inflammatory effects, and enhanced wound healing.

Subsequently, ELISA and western blot were used to detect changes in the levels of IL-10 and TNF-α during healing of the extraction wounds. Notably, IL-10 is a cytokine with an anti-inflammatory activity, while TNF-α is an important cytokine that contributes to the inflammatory response. Therefore, an effective anti-inflammatory therapy should promote the expression of IL-10 while suppressing the expression of TNF-α. As shown in Fig. 7b–e, the PNIPAM-TP and PNIPAM-TP/ICG hydrogels significantly increased the IL-10 levels and simultaneously decreased the TNF-α levels compared with control, although the difference between the two groups was not statistically significant. This suggests that the TPs exert a certain anti-inflammatory effect, whereas in the absence of laser irradiation, ICG exhibited no effect. However, the anti-inflammatory effect was enhanced in the PNIPAM-TP/ICG + laser group due to the PDT/PTT effect of ICG under laser irradiation. Overall, the above data confirm that PNIPAM-TP/ICG + laser treatment led to a strong anti-inflammatory effect caused by the anti-inflammatory effects of the TPs along with the sustained release of ICG and its ability to exert photothermal/photodynamic effects.

In addition, we also evaluated the systemic biotoxicity of the PNIPAM-TP/ICG hydrogel in SD rats. As shown in Table S1,† the main blood routine and liver function parameters of rats after being treated with hydrogel combined with or without laser irradiation maintained normal. For further histopathological analysis, the separated main organs (heart, liver, spleen, lung and kidney) were separated from SD rats after treatments and prepared to sections for H&E staining. As shown in Fig. S3,† the sections of main organs exhibited no damage and pathological changes. These results demonstrated that the therapeutic system we established based on PNIPAM hydrogel and laser irradiation possessed an excellent biosafety *in vivo*.

Conclusion

In this study, an innovative, injectable, and thermosensitive drug-loaded hydrogel that could accelerate the healing of infected extraction wounds was developed and prepared. This hydrogel acts by exhibiting enhanced haemostatic, antibacterial, and anti-inflammatory properties. More specifically, a tea polyphenol (TP)-modified poly-*N*-isopropylacrylamide (PNIPAM) hydrogel loaded with the photosensitiser indocyanine green (ICG) demonstrated a desirable structural integrity, injectability, and rheological properties. The loaded ICG was stably released into the oral environment to achieve photothermal and photodynamic effects, while the incorporation of TPs into the PNIPAM framework allowed for a sustained antibacterial action. Consequently, this hydrogel exhibited significant bacteriostatic effects against both *Porphyromonas gingivalis* and *Fusobacterium nucleatum*. Additionally, it demonstrated good haemostatic and anti-inflammatory properties, thereby promoting the healing of infected extraction wounds *in vivo*. This newly designed hydrogel possesses a good injectability, is easy to handle clinically, and exhibits potent haemostatic, anti-inflammatory, and antibacterial properties that accelerate the healing of extraction wounds. This hydrogel can therefore be considered a potential candidate for the treatment of various extraction wound infections, and it is expected that it will eventually be widely applied in clinical practice.

Conflicts of interest

The authors declare no competing financial interest.

Acknowledgements

This work was supported by the Tianjin Health Research Project (Grant No. TJWJ2021QN037 to S. S.) and the Science & Technology Development Fund of Tianjin Education Commission for Higher Education (Grant No. 2021KJ242 to S. S.). All animal procedures were performed in accordance with the Guidelines for Care and Use of Laboratory Animals of Tianjin Medical University and approved by the Animal Ethics Committee of Tianjin Medical University.

References

1 G. Chen, L. He, P. Zhang, J. Zhang, X. Mei, D. Wang, Y. Zhang, X. Ren and Z. Chen, *Mater. Sci. Eng., C*, 2020, **110**, 110686.
2 G. Lodi, L. Azzi, E. M. Varoni, M. Pentenero, M. Del Fabbro, A. Carrassi, A. Sardella and M. Manfredi, *Cochrane Database Syst. Rev.*, 2021, **2**, CD003811.
3 I. G. B. P. Santos, C. M. M. de Santana, A. T. N. N. Alves, M. J. P. G. de Uzeda, M. D. Calasans-Maia and R. B. de Santana, *J. Periodontol.*, 2019, **90**, 425–432.
4 H. Chen, G. Zhang, P. Weigl and X. Gu, *J. Prosthet. Dent.*, 2018, **120**, 658–667.
5 B. R. Chrcanovic, M. D. Martins and A. Wennerberg, *Clin. Implant Dent. Relat. Res.*, 2015, **17**, e1–e16.
6 W. Xu, Y. Sun, J. Wang, B. Wang, F. Xu, Z. Xie and Y. Wang, *RSC Adv.*, 2022, **12**, 13192–13202.
7 J. Xie, M. Zhou, Y. Qian, Z. Cong, S. Chen, W. Zhang, W. Jiang, C. Dai, N. Shao, Z. Ji, J. Zou, X. Xiao, L. Liu, M. Chen, J. Li and R. Liu, *Nat. Commun.*, 2021, **12**, 5898.
8 T. E. Brown and K. S. Anseth, *Chem. Soc. Rev.*, 2017, **46**, 6532–6552.
9 W. Huang, Y. Wang, Z. Huang, X. Wang, L. Chen, Y. Zhang and L. Zhang, *ACS Appl. Mater. Interfaces*, 2018, **10**, 41076–41088.

10 D. Bermejo-Velasco, S. Kadekar, M. V. Tavares da Costa, O. P. Oommen, K. Gamstedt, J. Hilborn and O. P. Varghese, *ACS Appl. Mater. Interfaces*, 2019, **11**, 38232–38239.
11 N. Golafshan, R. Rezahasani, M. Tarkesh Esfahani, M. Kharaziha and S. N. Khorasani, *Carbohydr. Polym.*, 2017, **176**, 392–401.
12 H. Huang, Y. Su, C. Wang, B. Lei, X. Song, W. Wang, P. Wu, X. Liu, X. Dong and L. Zhong, *ACS Appl. Mater. Interfaces*, 2023, **15**, 2714–2724.
13 M. Ma, Y. Zhong and X. Jiang, *Carbohydr. Polym.*, 2020, **236**, 116096.
14 Z. Guo, Z. Zhang, N. Zhang, W. Gao, J. Li, Y. Pu, B. He and J. Xie, *Bioact. Mater.*, 2022, **15**, 203–213.
15 X. Peng, Q. Peng, M. Wu, W. Wang, Y. Gao, X. Liu, Y. Sun, D. Yang, Q. Peng, T. Wang, X.-Z. Chen, J. Liu, H. Zhang and H. Zeng, *ACS Appl. Mater. Interfaces*, 2023, **15**, 19560–19573.
16 V. Roginsky and A. E. Alegria, *J. Agric. Food Chem.*, 2005, **53**, 4529–4535.
17 L. Basiricò, P. Morera, D. Dipasquale, R. Bernini, L. Santi, A. Romani, N. Lacetera and U. Bernabucci, *Animal*, 2019, **13**, 2847–2856.
18 L. Dong, Z. Han, H. Zhang, R. Yang, J. Fang, L. Wang, X. Li and X. Li, *Int. J. Biol. Macromol.*, 2022, **208**, 530–543.
19 L. Xing, H. Zhang, R. Qi, R. Tsao and Y. Mine, *J. Agric. Food Chem.*, 2019, **67**, 1029–1043.
20 A. K. Kar, A. Singh, N. Dhiman, M. P. Purohit, P. Jagdale, M. Kamthan, D. Singh, M. Kumar, D. Ghosh and S. Patnaik, *Int. J. Nanomed.*, 2019, **14**, 9837–9854.
21 Y. Shang, S. Smith and X. Hu, *Protein Cell*, 2016, **7**, 159–174.
22 Y.-W. Huang, Q.-Q. Zhu, X.-Y. Yang, H.-H. Xu, B. Sun, X.-J. Wang and J. Sheng, *FASEB J.*, 2019, **33**, 953–964.
23 S.-H. Kim, K. Kim, B. S. Kim, Y.-H. An, U.-J. Lee, S.-H. Lee, S. L. Kim, B.-G. Kim and N. S. Hwang, *Biomaterials*, 2020, **242**, 119905.
24 X. Xiong, J. Sun, D. Hu, C. Xiao, J. Wang, Q. Zhuo, C. Qin and L. Dai, *RSC Adv.*, 2020, **10**, 35226–35234.
25 T. Wu, C. Cui, C. Fan, Z. Xu, Y. Liu and W. Liu, *Bioact. Mater.*, 2021, **6**, 2820–2828.
26 C. Shi, J. B. Wu and D. Pan, *J. Biomed. Opt.*, 2016, **21**, 50901.
27 M. Pourhajibagher, N. Chiniforush, R. Raoofian, R. Ghorbanzadeh, S. Shahabi and A. Bahador, *Photodiagnosis Photodyn. Ther.*, 2016, **16**, 50–53.
28 M. Pourhajibagher, N. Chiniforush, R. Ghorbanzadeh and A. Bahador, *Photodiagnosis Photodyn. Ther.*, 2017, **17**, 61–64.
29 R. Fekrazad, K. Karamifar and A. Bahador, *Photodiagnosis Photodyn. Ther.*, 2016, **15**, 28–33.
30 M. Pourhajibagher, N. Chiniforush, S. Shahabi, R. Ghorbanzadeh and A. Bahador, *Photodiagnosis Photodyn. Ther.*, 2016, **15**, 159–166.
31 Z. Ni, J. Hu, Z. Ye, X. Wang, Y. Shang and H. Liu, *Mol. Pharm.*, 2022, **19**, 4527–4537.
32 H. Cui, D. Hu, J. Zhang, G. Gao, Z. Chen, W. Li, P. Gong, Z. Sheng and L. Cai, *ACS Appl. Mater. Interfaces*, 2017, **9**, 25114–25127.
33 W. Sun, L. Huang, Y. Yang, X. Liu and Z. Tong, *Chin. J. Polym. Sci.*, 2015, **33**, 70–83.
34 D. Zheng, C. Huang, Y. Hu, T. Zheng and J. An, *Colloids Surf., B*, 2022, **219**, 112831.
35 J. Qu, X. Zhao, Y. Liang, T. Zhang, P. X. Ma and B. Guo, *Biomaterials*, 2018, **183**, 185–199.